

PAPER

Electronic and crystal structures of $LnFeAsO_{1-x}H_x$ ($Ln = La, Sm$) studied by x-ray absorption spectroscopy, x-ray emission spectroscopy, and x-ray diffraction: II pressure dependence

To cite this article: Yoshiya Yamamoto *et al* 2021 *J. Phys.: Condens. Matter* **33** 255603

View the [article online](#) for updates and enhancements.



IOP | ebooks™

Bringing together innovative digital publishing with leading authors from the global scientific community.

Start exploring the collection—download the first chapter of every title for free.

Electronic and crystal structures of $LnFeAsO_{1-x}H_x$ ($Ln = La, Sm$) studied by x-ray absorption spectroscopy, x-ray emission spectroscopy, and x-ray diffraction: II pressure dependence

Yoshiya Yamamoto^{1,12}, Hitoshi Yamaoka^{2,*} , Takuma Kawai¹, Masahiro Yoshida¹, Jun-ichi Yamaura³ , Kenji Ishii⁴, Seiichiro Onari⁵, Takayuki Uozumi⁶, Atsushi Hariki⁶, Munetaka Taguchi⁷, Kensuke Kobayashi⁸, Jung-Fu Lin⁹, Nozomu Hiraoka¹⁰, Hirofumi Ishii¹⁰, Ku-Ding Tsuei¹⁰, Hiroshi Okanishi¹¹, Soshi Imura¹¹, Satoru Matsuishi¹¹, Hideo Hosono^{3,11} and Jun'ichiro Mizuki¹

¹ Graduate School of Science and Technology, Kwansai Gakuin University, Sanda, Hyogo 669-1337, Japan

² RIKEN SPring-8 Center, Sayo, Hyogo 679-5148, Japan

³ Materials Research Center for Element Strategy, Tokyo Institute of Technology, Yokohama, Kanagawa 226-8503, Japan

⁴ Synchrotron Radiation Research Center, National Institutes for Quantum and Radiological Science and Technology, Hyogo 679-5148, Japan

⁵ Department of Physics, Nagoya University, Chikusa, Nagoya 464-8602, Japan

⁶ Department of Physics and electronics, Osaka Prefecture University, 1-1 Gakuen, Nakaku, Sakai, Osaka 599-8531, Japan

⁷ Toshiba Nanoanalysis Corporation, Kawasaki, Kanagawa 212-8583, Japan

⁸ Institute of Materials Structure Science, High Energy Accelerator Research Organization (KEK), Tsukuba, Ibaraki 305-0801, Japan

⁹ Department of Geological Sciences, The University of Texas at Austin, Austin, Texas 78712, United States of America

¹⁰ National Synchrotron Radiation Research Center, Hsinchu 30076, Taiwan

¹¹ Laboratory for Materials and Structures, Tokyo Institute of Technology, Yokohama 226-8503, Japan

E-mail: yamaoka@spring8.or.jp

Received 31 January 2021, revised 31 March 2021

Accepted for publication 21 April 2021

Published 28 May 2021



CrossMark

Abstract

We examine electronic and crystal structures of iron-based superconductors $LnFeAsO_{1-x}H_x$ ($Ln = La, Sm$) under pressure by means of x-ray absorption spectroscopy (XAS), x-ray emission spectroscopy (XES), and x-ray diffraction. In $LaFeAsO$ the pre-edge peak on high-resolution XAS at the Fe- K absorption edge gains in intensity on the application of pressure up to 5.7 GPa and it saturates in the higher pressure region. We found integrated-absolute difference values on XES for $Ln = La$, corresponding to a spin state, decline on the application of pressure, and then it is minimized when the T_c approaches the maximum at around 5 GPa. In contrast, such the optimum value was not detected for

* Author to whom any correspondence should be addressed.

¹²Present address: Nagoya Institute of Technology, Gokiso, Showa, Nagoya, Aichi 466-8555, Japan

$Ln = Sm$. We reveal that the superconductivity is closely related to the lower spin state for $Ln = La$ unlike Sm case. We observed that As height from the Fe basal plane and As–Fe–As angle on the $FeAs_4$ tetrahedron for $Ln = La$ deviate from the optimum values of the regular tetrahedron in superconducting (SC) phase, which has been widely accepted structural guide to SC thus far. In contrast, the structural parameters were held near the optimum values up to ~ 15 GPa for $Ln = Sm$.

Keywords: pnictides and chalcogenides, iron superconductors, x-ray absorption spectra, high pressure, x-ray diffraction, electronic structure, crystal structure

 Supplementary material for this article is available [online](#)

(Some figures may appear in colour only in the online journal)

1. Introduction

Iron-based superconductors $LnFeAsO_{1-x}H_x$ ($Ln = La, Sm$), referred to as $Ln1111-H$, has unique phase diagrams with bipartite magnetic parent phases in the low- and high-electron doping regions and superconducting (SC) phases in between the parent phases [1–7]. $La1111-H$ has two SC dome with $T_{c,max} = 26$ K at $x \sim 0.08$ (SC1) and 37 K at $x \sim 0.35$ (SC2), while $Sm1111-H$ has a single SC dome with $T_{c,max} = 55$ K at $x \sim 0.2$. The electronic and crystal structures for $La1111-H$ and $Sm1111-H$ at ambient pressure were conducted in advance to the present study [8].

An application of pressure can drastically modify electronic structures without the degradation of the crystal against the chemical substitution. The high-pressure experiments have been providing guiding principles for the development of new superconductors and pave the way to promising new means of investigating iron-based superconductors. Takahashi *et al* have reported the pressure dependence of T_c up to 19 GPa for $Ln = La$ and Sm [9]. They especially observed the significant increase of T_c from 17 K at 0 GPa to 52 K at 6 GPa for $Ln = La$ at $x \sim 0.18$, corresponding to T_c -valley composition boundary of SC1 and SC2. Eventually, two SC domes were merged into the single SC one above 6 GPa. In contrast, T_c for $Ln = Sm$ decreased continually on the application of pressure with holding the single SC dome up to 15 GPa except for $x = 0$ [9]. Since the single SC dome for $Ln = La$ under pressure is similar to that for $Ln = Sm$, one might expect to find a certain common picture concerning the crystal and electronic structures between them.

In iron-based superconductors, an empirical guideline has been established that the superconductivity favored the regular tetrahedron crystal structure [10]; however the guideline was broken under pressure for $Ln = La$ [11]. Isovalent phosphorus substitution for $Sm1111-H$ gives rise to the splits of the single T_c dome into two domes gradually [12]. We thus expect that a certain criteria for structural parameters such as $Pn-Fe-Pn$ angle and electron-doping level are related to the superconductivity. One might care about the relation between the crystal structure and the superconductivity under pressure for $Ln = La$ and Sm ; in consequence the detail crystal structure

under pressure for $Ln1111-H$ warrants further investigation. Since in $Ln1111-H$ the magnetic parent phases are adjacent to the SC phases, we consider that the magnetic character is intimately tied to the superconductivity. The Fe spin state is known to correlate to the local magnetic moment and the superconductivity favors the higher spin state [13, 14]. Especially desirable but not yet to be performed is an investigation of the electronic structure including the spin state under pressure for $Ln = La$ and Sm .

In this paper we investigate electronic and crystal structures for $Ln = La, Sm$ under pressure by using x-ray emission spectroscopy (XES), high-resolution x-ray absorption spectroscopy (XAS), and x-ray diffraction (XRD) [15, 16]. We employed XAS with partial-fluorescence yield (PFY-XAS) at the Fe- K and As- K absorption edges [17, 18]. Fe $K\beta$ XES enables to probe the spin state of Fe d electrons under pressure [16, 19]. We found that the superconductivity is closely tied to the lower spin state for $Ln = La$ unlike Sm case. Moreover, in SC phase, the shape of $FeAs_4$ tetrahedron deviates from the regular tetrahedron for $Ln = La$, while it holds near the regular one for $Ln = Sm$. The regular tetrahedron of $FeAs_4$ is regarded as the optimum structure for emerging the high- T_c superconductivity in iron-based superconductors.

2. Experiments and methods

We prepared polycrystalline samples of $LaFeAsO_{1-x}H_x$ ($x = 0-0.51$) and $SmFeAsO_{1-x}H_x$ ($x = 0-0.65$) from high-pressure methods as reported in the literature [2]. The high-pressure measurements of XAS and XES were performed at BL12XU, SPring-8. The x-ray beam was focused to 20–30 (horizontal) \times 30–40 (vertical) μm^2 at the sample position using a toroidal and a K-B mirror. High-pressure conditions were achieved using a diamond anvil cell (DAC) coupled with a gas-membrane. A Be-gasket of 3 mm in diameter and approximately 100 μm thick was pre-indented to approximately 40 μm thickness around the center. The diameter of the sample chamber in the gasket was approximately 100–120 μm and the culet size of diamond anvil was 300 μm . KCl powder was used as a pressure medium for DAC. Both incoming and outgoing x-ray beams passed through the Be gasket

setting an in-plane geometry with the scattering angle of 90° . The Be gaskets (I-220-H grade) included an Fe impurity of $\sim 0.15\%$, giving rise to a background on the Fe $K\beta$ XES. The background was carefully reduced using a narrow slit system (the diameter of ~ 3 mm and the slit width of $30 \mu\text{m}$) [16]. The pressure was monitored by the ruby fluorescence method [20–22]. We performed the XRD measurements in the wide pressure ranges which cover the variable ranges of T_c for both compounds [11].

The Fe $K\beta$ XES exhibits main $K\beta_{1,3}$ and weak satellite $K\beta'$ components [23, 24]. In XES, an integrated-absolute difference (IAD) is strongly related to the spin state of d electrons and the magnetic moment [13, 14]. The IAD value was estimated from the Fe $K\beta$ XES based on the reference material FeCrAs without magnetic moment [19]. The detailed procedure of the analysis was described in our preceding paper [8].

The XRD image was taken using a three-pin plate DAC (Almax Industries) with a CCD detector. Both incoming and outgoing x-ray beams passed through the diamonds with the incident photon energy of 20 keV. NaCl powder as the pressure medium was carefully mixed with the sample to avoid the preferred orientation, and then the mixture was loaded to the gasket hole. The 2D image of CCD was integrated to yield the 2θ -intensity data by using FIT2D program [25]. The XRD patterns were analyzed by the Rietveld method on the RIETAN-FP program [26, 27]. All the above measurements were carried out at room temperature.

3. Results and discussion

3.1. PFY-XAS

Figures 1(a) and (e) show the pressure dependence of the PFY-XAS spectra for LaFeAsO ($x = 0$ of LaFeAsO $_{1-x}$ H $_x$) at the Fe- K and As- K absorption edges, respectively. Pressure-induced change in the electronic structure estimated by the observation of the Fe- K absorption edge was small. Figures 1(b) and (f) plot the XAS spectra near the Fe- K and As- K absorption edges, respectively. We fitted the PFY-XAS spectra for simplicity assuming some Voigt functions with an arctan-like background [8].

In figure 1(c) the relative intensity of the pre-edge peak (P1) estimated by the integration of the peak and the energy shift of P1 are shown. The intensity of the pre-edge peak increased with pressure up to 5.7 GPa and further increase of the pressure did not change the intensity. This behavior corresponds to the decrease of IAD values described below (see figure 2(e)). The peak energy of P1 was insensitive to the pressure in the entire pressure range.

Relative energy shifts of the absorption edges, which is defined as an inflection point at the Fe- K and As- K , are shown in figure 1(d). The Fe- K edge shifted monotonically to higher energy with pressure, while the As K edge did not show a clear pressure-induced change. The application of pressure causes a change in the Fe $4p$ DOS due to the volume contraction. Furthermore, the core-hole potential in the final states also affects the shape of the Fe $4p$ DOS largely. These effects are

superimposed, possibly resulting in the shift of the absorption edge.

The spectra at the As- K absorption edges changed significantly with pressure from 1.5 to 3.2 GPa as shown in figure 1(f). Such discontinuous change in the spectra at the As- K absorption edge has been observed at 0.6 GPa for BaFe $_2$ As $_2$ and Ba(Fe $_{0.92}$ Co $_{0.08}$) $_2$ As $_2$ and at 1.9 GPa for Ba $_{0.6}$ K $_{0.4}$ Fe $_2$ As $_2$ [28, 29]. The Ba122 system is believed that the pressure-induced change in the electronic structure of the As site is relatively large compared to that of the Fe site. Hereafter, we mention the relation between the Fe–As distance and the electronic structure. Balédent *et al* [28] found the electronic structure change at 2.39 Å in BaFe $_2$ As $_2$. We note the As–Fe distance reached to 2.39 Å at 1.4–2.6 GPa in LaFeAsO $_{1-x}$ H $_x$ ($x = 0$) [31]. The results suggest that the pressure-induced change in the electronic structure of As is more important than that of Fe in the emergence of the superconductivity in LaFeAsO as observed in Ba122 systems.

At the As- K absorption edge the pressure-induced change in the intensity and energy of the P4, P5, and P6 peaks probably corresponds to the change in the As $4p$ DOS as observed in literature [28]. The intensities of these peaks do not show the clear pressure dependence as shown in figure 1(g). While these energies of them increased with pressure up to 7.8 GPa as shown in figure 1(h) and the change in the energy was gentle with further increase of the pressure. The energy change is coincided with a fact that T_c increases up to ~ 5 GPa, and then it saturates in the higher pressure range.

We measured the pressure dependence of the PFY-XAS spectra of SmFeAsO $_{1-x}$ H $_x$ at the Fe- K and the As- K absorption edges for $x = 0, 0.22,$ and 0.59 [31]. In SmFeAsO $_{1-x}$ H $_x$, however, no significant correlation has been observed between the superconductivity and the electronic structure under pressure.

3.2. $K\beta$ XES

The pressure dependence of the Fe $K\beta$ XES spectra of LaFeAsO $_{1-x}$ H $_x$ for $x = 0.07$ at SC 1 and 0.35 at SC 2 with a spectrum of FeCrAs are shown in figures 2(a) and (b) with the difference of the intensity for FeCrAs in figures 2(c) and (d). The IAD values are estimated as shown in figure 2(e). The IAD values of both samples decreased rapidly up to 5 GPa with pressure, and that of the $x = 0.35$ sample had a trend to increase once with further increase of the pressure. The pressure dependence of the IAD values of the 0.35 sample showed an inverse correlation with T_c as shown in figure 2(e). It was reported that the magnetic order of polycrystalline LaFeAsO sample remained up to 20 GPa [32]. Thus, by considering that the application of pressure increases the hybridization between Fe- d and As- p orbitals, it is naturally understood that the local magnetic moment decreases under pressure. For an example, in FeSe the IAD values decreased with pressure monotonically [33, 34]. Thus, the slight increase of the IAD values of the $x = 0.35$ sample at high pressures is anomalous. Such the pressure-induced anomalous behavior of IAD has been observed in the 122 systems of K $_x$ Fe $_{2-y}$ Se $_2$ and (NH $_3$) $_y$ Cs $_{0.4}$ FeSe [35, 36], which have two pressure-induced

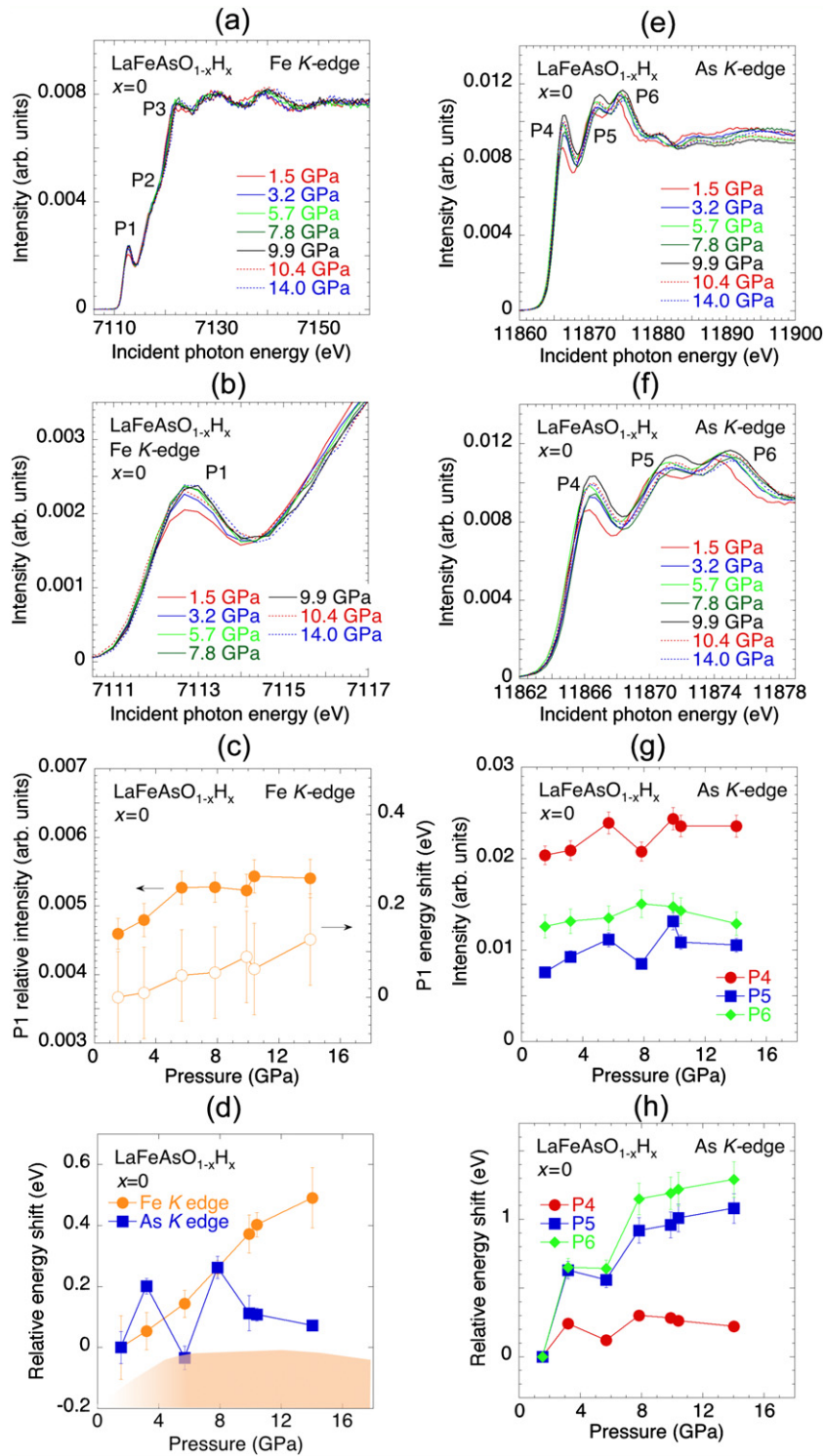


Figure 1. (a) Pressure dependence of the PFY-XAS spectra at the Fe-K absorption edge for $\text{LaFeAsO}_{1-x}\text{H}_x$ ($x=0$). (b) Expanded view of (a) near the pre-edge peak. (c) Pressure dependence of the relative intensity and energy shift of the pre-edge peak P1 at the Fe-K absorption edge. (d) Pressure dependence of the relative energy shifts of the Fe-K and As-K absorption edges. (e) Pressure dependence of the PFY-XAS spectra at the As-K absorption edge for $\text{LaFeAsO}_{1-x}\text{H}_x$ ($x=0$). (f) Expanded view of (e) near the absorption edge. (g) Pressure dependence of the intensity of the peaks P4, P5, and P6. (h) Pressure dependence of the relative energy shifts of the peaks P4, P5, and P6. Pink-colored area in (d) correspond to the SC regions for $x=0$, where the maximum value of the vertical axis scales linearly to be 90 K from 0 K [30].

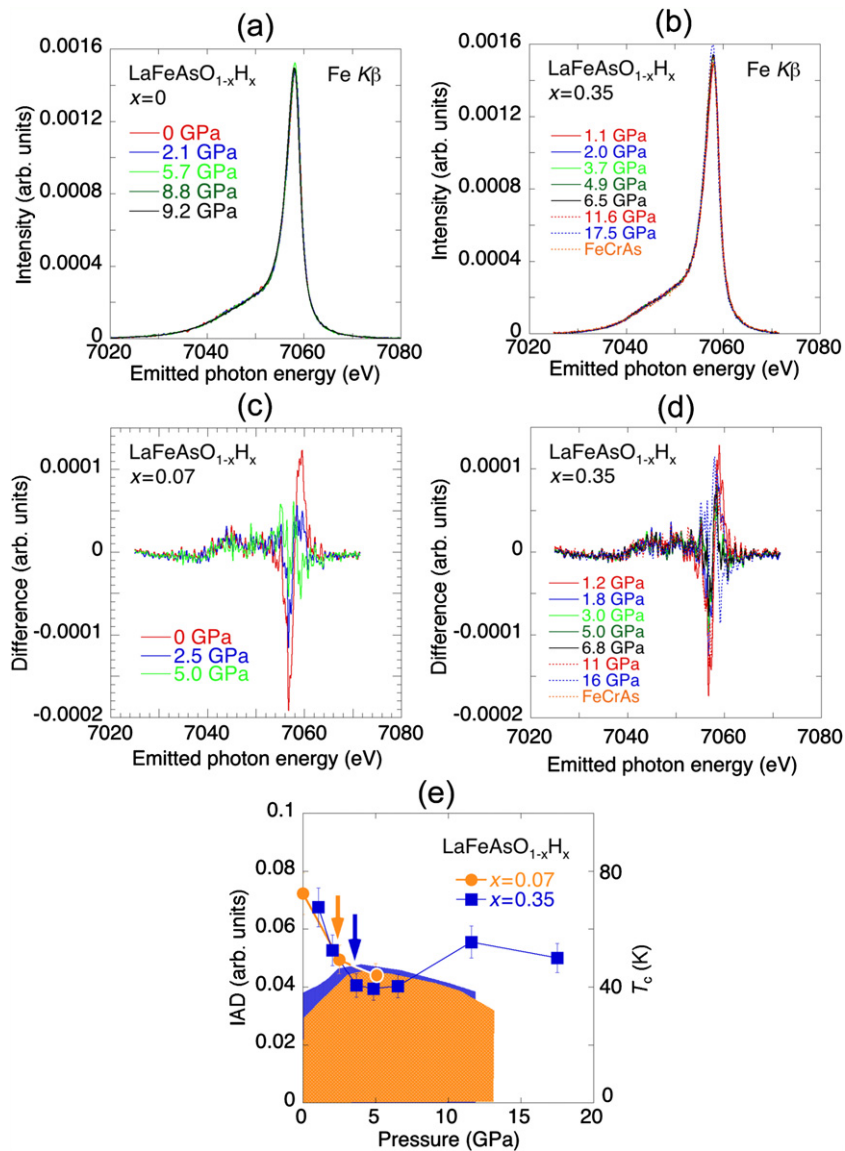


Figure 2. (a) and (b) Pressure dependence of the Fe $K\beta$ XES spectra of $\text{LaFeAsO}_{1-x}\text{H}_x$ for (a) $x = 0.07$ and (b) $x = 0.35$ with a spectrum of FeCrAs. (c) and (d) Pressure dependence of the difference of the intensity between the Fe $K\beta$ XES spectra of $\text{LaFeAsO}_{1-x}\text{H}_x$ and the spectrum of FeCrAs for (c) $x = 0.07$ and (d) $x = 0.35$. (e) Pressure dependence of the IAD values for $x = 0.07$ and $x = 0.35$. Pink- and blue-colored areas in (e) correspond to the SC regions (T_c) for $x = 0.07$ and 0.35 , respectively, where the maximum value of the right vertical axis scales linearly to be 100 K from 0 K [2, 5]. The pressures where the Fe–As interatomic distance is 2.39 Å are shown by arrows.

SC domes of SC 1 and SC 2 [37, 38]. However, in the $x = 0.35$ sample of $\text{LaFeAsO}_{1-x}\text{H}_x$ it seems not to show the emergence of SC 2 induced by pressure, while T_c decreases at high pressure [9, 31]. In the 122 system, the pressure often induces the collapsed tetragonal structure, which triggers the emergence of second SC phase. However, such the collapsed phase was not observed in $\text{LaFeAsO}_{1-x}\text{H}_x$. Our results suggest that in $\text{LaFeAsO}_{1-x}\text{H}_x$ the minimum IAD value (i. e. spin state) of 0.04 matches the maximum T_c , as observed in figure 2(e); thus the superconductivity seems to favor the lower magnetic moment. Additionally, in $\text{LaFeAsO}_{1-x}\text{H}_x$ the x dependence of the superconductivity forms the single SC dome with the maximum T_c at 6 GPa [11]. Therefore, our results also suggest that the pressure can induce the optimum conditions to emerge the high- T_c superconductivity in $\text{LaFeAsO}_{1-x}\text{H}_x$.

There is a possible explanation of the IAD anomaly based on the band calculations of LaFeAsO by Harada *et al* [39] They reported that the distributions of the charge density decrease on Fe $d_{3z^2-r^2}$ and d_{zx} and increase on Fe $d_{x^2-y^2}$ with pressure, resulting in the Fe d -states accumulation rearranged through the hybridization between the Fe- d and As- p states. The accumulation around the Fe site reaches the maximum at 4 GPa, and the distribution gradually spreads toward the outside of Fe with further increase of the pressure. This indicates that the bonding of Fe–As becomes weak above 4 GPa, although the Fe–As distance decreases monotonically with pressure. Therefore, the slight increase of the IAD value above 5 GPa of the $x = 0.35$ sample may correlate to the gradual spread of the charge distribution around the Fe site. These pressure-induced

behaviors of the IAD and the strength of the Fe–As bond also correspond to the pressure dependence of T_c [9, 31].

Hesani and Yazdani performed DFT + DMFT calculations of LaFeAsO under pressure [40]. The pressure effect on the Fe 3*d*-orbital occupation number enhanced the charge transfer from $d_{x^2-y^2}$ to other orbitals. The occupation number increases on the d_{xy} orbital and decreases on the $d_{x^2-y^2}$ up to ~ 13 GPa. The total occupation number of Fe 3*d* also increased up to around 13 GPa. The pressure dependence of these occupation numbers kept the similar trend with further increase of the pressure up to 34 GPa albeit those pressure-induced change are small.

These behaviors of the *d*-orbital occupation numbers are correlated to the pressure dependence of T_c . On the other hand, Iimura *et al* showed that in LaFeAsO_{1-x}H_x the energy of the anti- d_{xy} orbital decreased with *x* and the degeneration of the orbitals of anti- d_{xy} , $d_{yz,xz}$, and d_{xy} occurred. The application of pressure moreover decreases the As–Fe distance with increasing the hybridization, while the electron doping elongates the As–Fe distance with increasing the *x*. The pressure is likely to change the energy levels of the d_{xy} orbital similar to the case of the electron doping.

Figures 3(a), (c) and (e) show pressure dependence of the Fe $K\beta$ XES spectra of SmFeAsO_{1-x}H_x for *x* = 0, 0.22, and 0.59 with the difference of the intensity for the spectrum of FeCrAs in figures 3(b), (d) and (f), respectively. The application of pressure decreased the IAD values; especially the decrease of IAD at *x* = 0.59 was significantly larger than that at *x* = 0, as shown in figure 3(g). The IAD values of SmFeAsO_{1-x}H_x were larger than those of LaFeAsO_{1-x}H_x. The IAD value at *x* = 0.22 indicated a rapid increase at the first pressurization to 1.2 GPa, in which the Fe–As distance reaches the transition value of As state to be 2.39 Å from the XRD data. At ambient pressure the *x* = 0 sample of SmFeAsO_{1-x}H_x does not show the superconductivity [31]. However, a small amount of the carrier doping suppressed the AFM order and induced the superconductivity as with LaFeAsO_{1-x}H_x. The 7%-hydrogen substitution involved the high- T_c superconductivity at around 50 K and the application of pressure decreased T_c , although the available data of T_c for *x* > 0 was limited below 2.5 GPa in the previous reports [31, 41, 42]. In SmFeAsO_{1-x}H_x there was no IAD anomaly as observed in the *x* = 0.35 sample of LaFeAsO_{1-x}H_x. The IAD values decreased gradually in the high-pressure range. The observations are considered as the ordinary characters of IAD along with the decreases of local magnetic moments because the application of pressure makes the band broadened. In SmFeAsO_{1-x}H_x the IAD values of the *x* = 0.22 sample are probably correlated to T_c under high pressures. The highest T_c was observed at around *x* = 0.22 [9, 31], in which the tetrahedron of FeAs₄ involves the regular shape in the entire pressure range measured as will be shown in later. In SmFeAsO_{1-x}H_x the higher T_c favors the higher spin state, in contrast to the case of LaFeAsO_{1-x}H_x.

Balédent *et al* [28] suggested a critical Fe–As interatomic distance of 2.39 Å in the Fe122 systems; below this distance the hybridization was strong enough to enable the redistribution of the charge between Fe and As orbitals resulting in sudden changes in the As electronic structure. In figures 2(e)

and 3(g) the pressures where the Fe–As interatomic distance is 2.39 Å are shown by arrows. In the *x* = 0.22 sample of SmFeAsO_{1-x}H_x the IAD values also seem to change rapidly around above pressures.

3.3. Crystal structure

The pressure dependence of diffraction patterns, lattice constants, ratio of *c/a*, As heights, As–Fe–As angles and As–Fe distances of LaFeAsO_{1-x}H_x and SmFeAsO_{1-x}H_x are summarized in the supplementary information (<https://stacks.iop.org/JPCM/33/265602/mmedia>) [31]. There is no structural phase transition in the pressure range measured in both La and Sm systems. In LaFeAsO_{1-x}H_x the lattice constants of *a* and *c* decreased monotonically with applying the pressure or increasing *x*. The ratio of *c/a* decreased monotonically with pressure and no anomaly was observed for all doping levels (figure S5(a)) [31]. The ratio showed an increase with *x*, indicating the elongation along the *c* axis with *x*. In LaFeAsO_{1-x}H_x the As height deviated from the ideal value of ~ 1.38 Å and the pressure squeezed the FeAs₄ tetrahedron along the *c*-axis, leading to the decrease of As height (figure S5(b)) [10, 31, 43]. The As–Fe–As angle 1 also increased and deviated from the ideal value with pressure (figure S5(c)), while the angle 2 (figure S5(d)) showed an opposite trend. Our results agree with the reported data previously [1, 9, 11], but our measurements could approach at the higher pressure range. It has been considered that the superconductivity favored the regular tetrahedron of FeAs₄ [10, 43] since the discovery of iron-based superconductor [44]. However, in LaFeAsO_{1-x}H_x the high T_c was observed even in the pressure range where the FeAs₄ shape deviates from the ideal one. The As height decreased rapidly with pressure for all samples. The As height at *x* = 0.51 reached the ideal value of 1.38 Å at around 3–4 GPa, however T_c at *x* = 0.44 decreased monotonically with pressure. These results suggest that the crystal structure in LaFeAsO_{1-x}H_x could be less important for the emergence of the superconductivity compared to the other iron-based superconductors.

The pressure dependence of the lattice constants of SmFeAsO_{1-x}H_x was similar to those of LaFeAsO_{1-x}H_x. [31] The ratio *a/c* (figure S5(f)) and the lattice constants of *a* and *c* decreased monotonically with applying the pressure and increasing *x* [1, 9]. In SmFeAsO_{1-x}H_x the As heights of these samples laid near the ideal value up to ~ 15 GPa and decreased slightly with pressure. The As–Fe–As angles were near the ideal value at low pressure, however they deviated at higher pressures. These results in SmFeAsO_{1-x}H_x are in contrast to those in LaFeAsO_{1-x}H_x, where the large deviation of the FeAs₄ tetrahedron from the regular one was observed as described above.

The pressure dependence of the lattice constants indicated the change of the trend at around 10 GPa [31], namely the compressibility along the *a* axis became smaller as the pressure increased. The pressure dependence of the As height and As–Fe–As angles also showed the change in the trend at around the same pressure range [31]. In the samples except for *x* = 0.44, T_c took maximum at around the pressure range

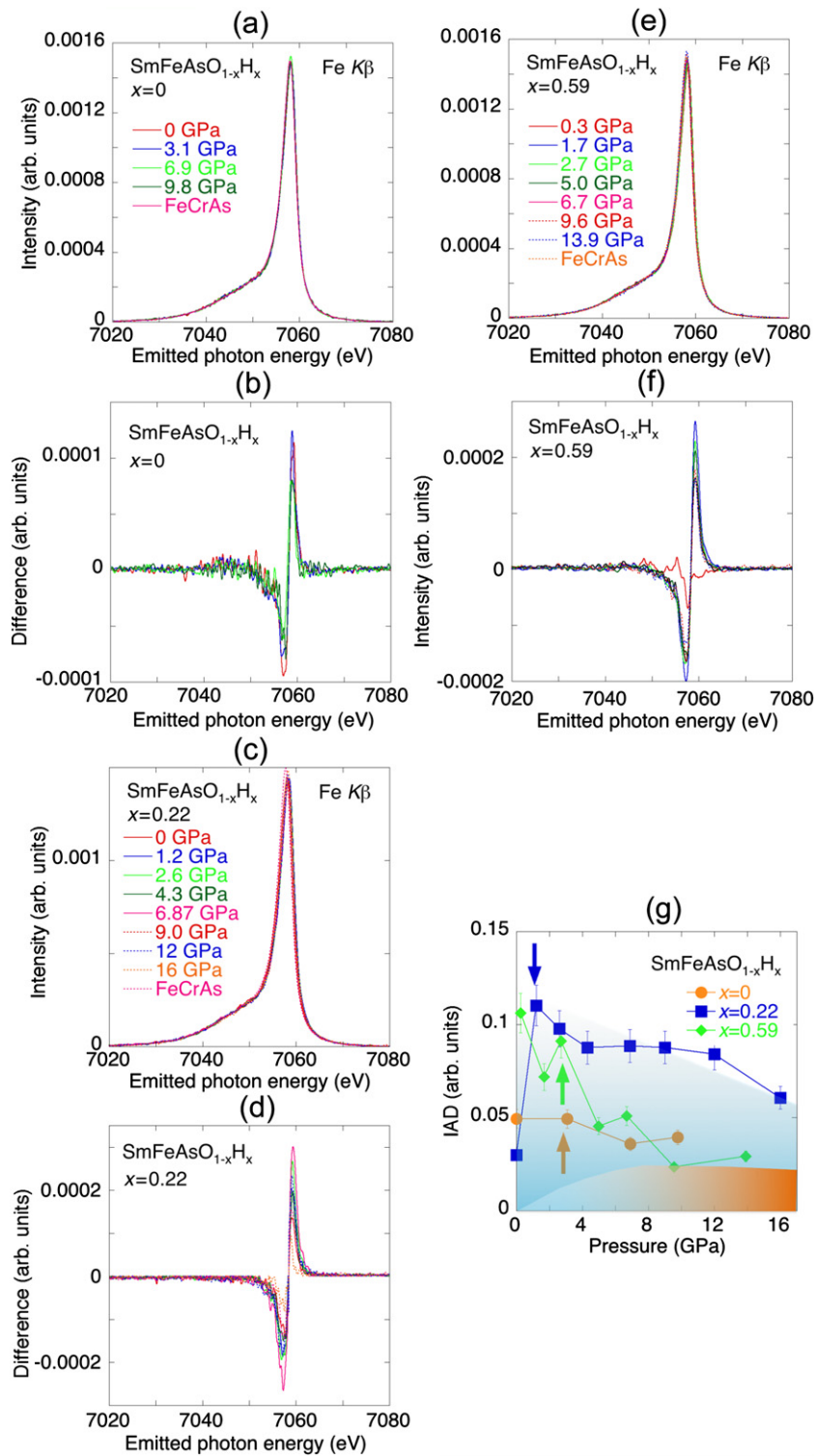


Figure 3. (a)–(f) Pressure dependence of the Fe $K\beta$ XES spectra of $\text{SmFeAsO}_{1-x}\text{H}_x$ for (a) $x = 0$, (c) $x = 0.22$, and (e) $x = 0.59$ with the difference of the intensity between the Fe $K\beta$ XES spectra of $\text{LaFeAsO}_{1-x}\text{H}_x$ and the spectrum of FeCrAs for (b) $x = 0$, (d) $x = 0.22$, and (f) $x = 0.59$. (g) Pressure dependence of the IAD values for $x = 0$, $x = 0.22$, and $x = 0.59$. Pink- and blue-colored areas in (g) correspond to the SC regions for $x = 0$ and $x = 0.22$, respectively, where the maximum value of the vertical axis scales linearly to be 60 K from 0 K [9, 41]. The pressures where the Fe–As interatomic distance is 2.39 Å are shown by arrows [28]. Pink- and turquoise-blue colored areas in (g) correspond to the SC regions for $x = 0$ and 0.22, respectively, where the maximum value of the vertical axis scales linearly to be 60 K from 0 K [9, 41]. Note that the pressure dependence of T_c of the $x = 0.59$ sample has not been measured.

[31] and the further increase of pressure decreased T_c . There may be an optimum crystal structure for high- T_c lies within the above pressure range in $\text{SmFeAsO}_{1-x}\text{H}_x$. The As–Fe distances are longer than the critical value of 2.39 Å at ambient pressure for three Sm samples, and then they passed through the critical value in the low pressure range of 1–2 GPa [31] as observed in the Fe122 systems [28, 29].

The ratio of c/a has been relatively higher at $x = 0.35$ of $\text{LaFeAsO}_{1-x}\text{H}_x$ and at $x = 0.22$ of $\text{SmFeAsO}_{1-x}\text{H}_x$ in the whole pressure range measured. Since the superconductivity was observed up to ~ 20 GPa for both $\text{LaFeAsO}_{1-x}\text{H}_x$ and $\text{SmFeAsO}_{1-x}\text{H}_x$, present superconductivity favors the relatively larger c/a ratio.

In figures 4(a) and (b) we summarize the pressure dependence of the representative structural parameters along with the contour plots of T_c as a function of the As–Fe–As bond angle and the Fe–As distance. In $\text{SmFeAsO}_{1-x}\text{H}_x$ the data of T_c are not available at medium pressure range above a few GPa [31] and those data are interpolated or extrapolated in figure 4(b) to connect smoothly to the data measured. In $\text{LaFeAsO}_{1-x}\text{H}_x$ the present results reproduced well the previous data by Kobayashi *et al* [11]. It is clearly shown that the superconductivity occurred at the wide pressure ranges deviated largely from the ideal As–Fe–As bond angle and the Fe–As distance in $\text{LaFeAsO}_{1-x}\text{H}_x$. It was reported that the AFM2 phase at $x > 0.5$ in $\text{LaFeAsO}_{1-x}\text{H}_x$ was suppressed at around 6 GPa, while the AFM phase existed at the same pressure range [11]. The As height from the Fe plane increased with increasing x in $\text{LaFeAsO}_{1-x}\text{H}_x$. The application of pressure decreased the As height and it should increase the hybridization between the Fe and As orbitals.

On the other hand, in $\text{SmFeAsO}_{1-x}\text{H}_x$ we found that the superconductivity was observed when the As–Fe–As angle and the Fe–As distance approached the ideal values. In $\text{LaFeAsO}_{1-x}\text{H}_x$ the electron doping effectively changes the crystal structure from the ideal ones. In $\text{SmFeAsO}_{1-x}\text{H}_x$ slight increase of the pressure from the ambient pressure caused a collapse along all axes at $x = 0.22$. This may be correspond to the sudden increase of the IAD values at 1.2 GPa of the $x = 0.22$ sample in figure 3(g) described above. The $x = 0.2$ sample of $\text{SmFeAsO}_{1-x}\text{H}_x$ laid near the pressure range with the regular tetrahedron of FeAs_4 compared to the other samples in the all pressure range as shown in figure 4(b). This may be a reason why T_c of the $x = 0.2$ sample is always higher than those of other samples in $\text{SmFeAsO}_{1-x}\text{H}_x$ [31]. At the overdoping sample of $x = 0.65$ the lattice easily shrinks along the a and b axes.

$\text{LaFeAsO}_{1-x}\text{H}_x$ deviated largely from the As–Fe–As angle of 109.5° . On the other hand, the substitution from La to Sm made the Fe–As distance in the Sm systems shorten owing to the lanthanoid contraction. In $\text{SmFeAsO}_{1-x}\text{H}_x$ the crystal structure had the ideal characters of the As–Fe–As angle and the Fe–As distance at ambient pressure. The application of pressure induced the deviations from the ideal values of the As–Fe–As angle and the Fe–As distance, however the deviation was not large at least up to ~ 15 GPa compared to the case of the La system at ambient pressure.

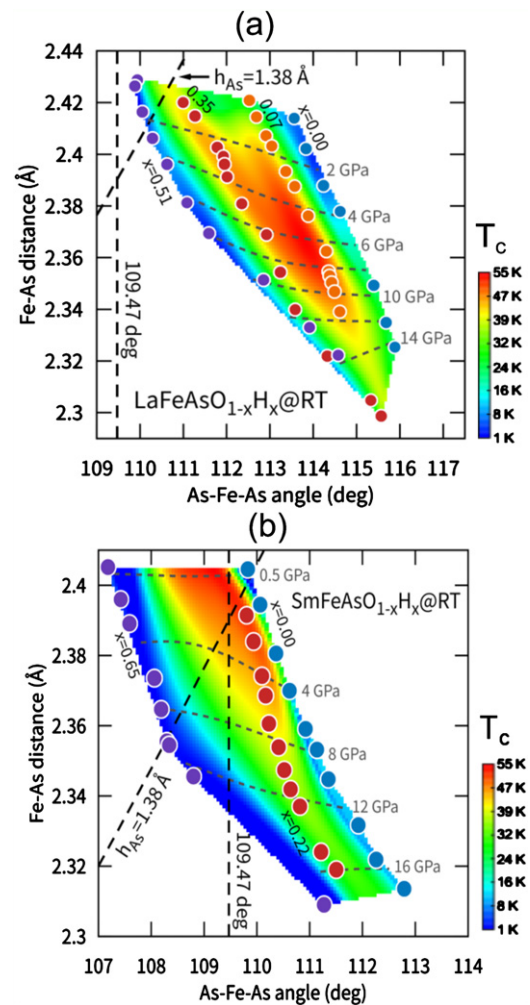


Figure 4. Contour plots of T_c for (a) $\text{LaFeAsO}_{1-x}\text{H}_x$ and (b) $\text{SmFeAsO}_{1-x}\text{H}_x$ as a function of the As–Fe–As bond angle and the Fe–As distance. Broken lines represent the regular tetrahedron and the As height.

Theoretical calculations showed in $\text{SmFeAsO}_{1-x}\text{H}_x$ a larger hole-type Fermi surface at M point and better nesting condition than the La case, resulting a single dome superconductivity with the hydrogen doping in $\text{SmFeAsO}_{1-x}\text{H}_x$ at ambient pressure [8]. However, in $\text{LaFeAsO}_{1-x}\text{H}_x$ the nesting is observed at all hydrogen doping range. It is expected that such nesting condition may be kept in $\text{LaFeAsO}_{1-x}\text{H}_x$ even under pressure where the crystal structure is far from the regular tetrahedron. It remains as an issue to be challenged in the future theoretically.

4. Conclusion

Pressure dependence of electronic and crystal structures of $\text{LnFeAsO}_{1-x}\text{H}_x$ ($\text{Ln} = \text{La}, \text{Sm}$) studied in detail. Pressure decreased the IAD values for both La and Sm systems, except for the $x = 0.35$ of the La system where the IAD values increased at high pressures. In $\text{LaFeAsO}_{1-x}\text{H}_x$ pressure dependence of the IAD values showed there is an optimum value (i. e. spin state), where highest T_c was observed under pressure.

This suggest that the superconductivity favors the low-spin state under pressure near the AFM1 range in $\text{LaFeAsO}_{1-x}\text{H}_x$. The slight increase of the IAD value above 5 GPa of the $x = 0.35$ sample is probably correlated to the gradual spread of the charge distribution around the Fe site. Our study has revealed the importance of the hybridization between Fe- d and As- p orbitals to control the T_c . This suggests that it is not necessary to have the regular tetrahedron of FeAs_4 shape for searching high- T_c materials.

The As height from Fe-plane and As–Fe–As angle deviated from the optimum values of the regular tetrahedron crystal structure for the emergence of the superconductivity, which have been accepted widely so far, with pressure in $\text{LaFeAsO}_{1-x}\text{H}_x$. In $\text{LaFeAsO}_{1-x}\text{H}_x$ the crystal structure deviated from the regular FeAs_4 tetrahedron crystal structure in a wide pressure range measured. While in $\text{SmFeAsO}_{1-x}\text{H}_x$ the deviation from the regular tetrahedron crystal structure caused the decrease of T_c . We found that As height from Fe-plane and As–Fe–As angle were kept near the optimum values up to around 15 GPa in $\text{SmFeAsO}_{1-x}\text{H}_x$.

Acknowledgments

The experiments were performed BL12XU, and BL12B2, SPring-8 under SPring-8 Proposal Nos. 2014B4131, 2014B4256, 2014B4268, 2016A4137, and 2017A4255 (corresponding to NSRRC Proposal Nos. 2014-3-004, 2016-1-013, and 2017-1-656 for BL12XU and BL12B2). The experiments at BL11XU, SPring-8 were performed under SPring-8 Proposal No. 2013A3502. The work was supported by Grants in Aid for Scientific Research from the Japan Society for the Promotion of Science, KAKENHI 15K05194, and by MEXT Elements Strategy Initiative to Form Core Research Center, No. JPMXP0112101001. We thank Masahito Kurooka in Kwansai Gakuin University for his help in the experiment at BL11XU.

Data availability statement

All data that support the findings of this study are included within the article (and any supplementary files).

ORCID iDs

Hitoshi Yamaoka  <https://orcid.org/0000-0003-0462-5385>

Jun-ichi Yamaura  <https://orcid.org/0000-0002-8992-9099>

References

- [1] Hosono H and Matsuishi S 2013 Superconductivity induced by hydrogen anion substitution in 1111-type iron arsenides *Curr. Opin. Solid State Mater. Sci.* **17** 49
- [2] Iimura S, Matsuishi S, Sato H, Hanna T, Muraba Y W, Kim S W, Kim J E, Takata M and Hosono H 2013 Two-dome structure in electron-doped iron arsenide superconductors *Nat. Commun.* **3** 943
- [3] Iimura S *et al* 2013 Switching of intra-orbital spin excitations in electron-doped iron pnictide superconductors *Phys. Rev. B* **88** 060501(R)
- [4] Fujiwara N, Iimura S, Matsuishi S, Hosono H, Yamakawa Y and Kontani H 2014 NMR study on a pnictide superconductor $\text{LaFeAsO}_{1-x}\text{H}_x$ in a H-overdoped regime: revival of antiferromagnetic fluctuations *J. Supercond. Nov. Magn.* **27** 933
- [5] Hiraishi M *et al* 2014 Bipartite magnetic parent phases in the iron oxypnictide superconductor *Nat. Phys.* **10** 300
- [6] Iimura S, Matsuishi S and Hosono H 2016 Heavy electron doping induced antiferromagnetic phase as the parent for the iron oxypnictide superconductor $\text{LaFeAsO}_{1-x}\text{H}_x$ *Phys. Rev. B* **94** 024512
- [7] Iimura S and Hosono H 2020 Heavily hydride-ion-doped 1111-type iron-based superconductors: synthesis, physical properties and electronic structure *J. Phys. Soc. Japan* **89** 051006
- [8] Yamamoto Y *et al* 2021 Electronic and crystal structures of $\text{LnFeAsO}_{1-x}\text{H}_x$ ($\text{Ln} = \text{La}, \text{Sm}$) studied by x-ray absorption spectroscopy, x-ray emission spectroscopy, and x-ray diffraction: I carrier-doping dependence *J. Phys.: Condens. Matter.* <https://doi.org/10.1088/1361-648X/abf9b9>
- [9] Takahashi H, Soeda H, Nukii M, Kawashima C, Nakanishi T, Iimura S, Muraba Y, Matsuishi S and Hosono H 2015 Superconductivity at 52 K in hydrogen-substituted $\text{LaFeAsO}_{1-x}\text{H}_x$ under high pressure *Sci. Rep.* **5** 7829
- [10] Lee C-H *et al* 2008 Effect of structural parameters on superconductivity in fluorine-free LnFeAsO_{1-y} ($\text{Ln} = \text{La}, \text{Nd}$) *J. Phys. Soc. Japan* **77** 083704
- [11] Kobayashi K *et al* 2016 Pressure effect on iron-based superconductor $\text{LaFeAsO}_{1-x}\text{H}_x$: peculiar response of 1111-type structure *Sci. Rep.* **6** 39646
- [12] Matsuishi S, Maruyama T, Iimura S and Hosono H 2014 Controlling factors of T_c dome structure in 1111-type iron arsenide superconductors *Phys. Rev. B* **89** 094510
- [13] Gretarsson H *et al* 2011 Revealing the dual nature of magnetism in iron pnictides and iron chalcogenides using x-ray emission spectroscopy *Phys. Rev. B* **84** 100509(R)
- [14] Gretarsson H *et al* 2013 Spin-state transition in the Fe pnictides *Phys. Rev. Lett.* **110** 047003
- [15] Rueff J-P and Shukla A 2010 Inelastic x-ray scattering by electronic excitations under high pressure *Rev. Mod. Phys.* **82** 847
- [16] Yamaoka H 2016 Pressure dependence of the electronic structure of 4f and 3d electron systems studied by x-ray emission spectroscopy *High Press. Res.* **36** 262
- [17] Hämäläinen K, Siddons D P, Hastings J B and Berman L E 1991 Elimination of the inner-shell lifetime broadening in x-ray-absorption spectroscopy *Phys. Rev. Lett.* **67** 2850
- [18] Hämäläinen K, Kao C-C, Hastings J B, Siddons D P, Berman L E, Stojanoff V and Cramer S P 1992 Spin-dependent x-ray absorption of MnO and MnF_2 *Phys. Rev. B* **46** 14274
- [19] Vankó G, Neisius T, Molnár G, Renz F, Kárpáti S, Shukla A and de Groot F M F 2006 Probing the 3d spin momentum with x-ray emission spectroscopy: the case of molecular-spin transitions *J. Phys. Chem B* **110** 11647
- [20] Mao H K and Bell P M 1976 High-pressure physics: the one-megabar mark on the ruby R1 static pressure scale *Science* **191** 851
- [21] Syassen K 2008 Ruby under pressure *High Press. Res.* **28** 75

- [22] Yamaoka H, Zekko Y, Jarrige I, Lin J-F, Hiraoka N, Ishii H, Tsuei K-D and Mizuki J i 2012 Ruby pressure scale in a low-temperature diamond anvil cell *J. Appl. Phys.* **112** 124503
- [23] Tsutsumi K 1959 The x-ray non-diagram lines $K\beta'$ of some compounds of the iron group *J. Phys. Soc. Japan* **14** 1696
- [24] Tsutsumi K, Nakamori H and Ichikawa K 1976 X-ray $MnK\beta$ emission spectra of manganese oxides and manganates *Phys. Rev. B* **13** 929
- [25] Hammersley A P, Svensson S O, Hanfland M, Fitch A N and Hausermann D 1996 Two-dimensional detector software: from real detector to idealised image or two-theta scan *High Press. Res.* **14** 235
- [26] Momma K and Izumi F 2008 VESTA: a three-dimensional visualization system for electronic and structural analysis *J. Appl. Crystallogr.* **41** 653
- [27] Izumi F and Momma K 2007 Three-dimensional visualization in powder diffraction *Solid State Phenom.* **130** 15
- [28] Balédent V, Rullier-Albenque F, Colson D, Ablett J M and Rueff J-P 2015 Electronic properties of $BaFe_2As_2$ upon doping and pressure: the prominent role of the as p orbitals *Phys. Rev. Lett.* **114** 177001
- [29] Yamaoka H *et al* 2017 Electronic structures and spin states of $BaFe_2As_2$ and $SrFe_2As_2$ probed by x-ray emission spectroscopy at Fe and As K -absorption edges *Phys. Rev. B* **96** 085129
- [30] Okada H, Igawa K, Takahashi H, Kamihara Y, Hirano M, Hosono H, Matsubayashi K and Uwatoko Y 2008 Superconductivity under high pressure in $LaFeAsO$ *J. Phys. Soc. Japan* **77** 113712
- [31] See supplementary information. Pressure dependence of the PFY-XAS spectra of $SmFeAsO_{1-x}H_x$, the results of the XRD under pressure, and pressure dependence of T_c with a table of the pressures, where the Fe-As interatomic distance is 2.39 Å, are shown, including references [1, 9–11, 28, 30, 41–47].
- [32] Kumar R S *et al* 2014 Pressure-induced superconductivity in $LaFeAsO$: the role of anionic height and magnetic ordering *Appl. Phys. Lett.* **105** 251902
- [33] Chen J M *et al* 2011 Pressure dependence of the electronic structure and spin state in $Fe_{1.01}Se$ superconductors probed by x-ray absorption and x-ray emission spectroscopy *Phys. Rev. B* **84** 125117
- [34] Kumar R S, Zhang Y, Xiao Y, Baker J, Cornelius A, Veeramalai S, Chow P, Chen C and Zhao Y 2011 Pressure induced high spin-low spin transition in $FeSe$ superconductor studied by x-ray emission spectroscopy and *ab initio* calculations *Appl. Phys. Lett.* **99** 061913
- [35] Yamamoto Y *et al* 2016 Origin of pressure-induced superconducting phase in $K_xFe_{2-y}Se_2$ studied by synchrotron x-ray diffraction and spectroscopy *Sci. Rep.* **6** 30946
- [36] Yamamoto Y *et al* 2019 Study of the pressure-induced second superconducting phase of $(NH_3)_yCs_{0.4}FeSe$ with double-dome superconductivity *J. Phys. Soc. Japan* **88** 074704
- [37] Sun L *et al* 2012 Re-emerging superconductivity at 48 kelvin in iron chalcogenides *Nature* **483** 67
- [38] Zheng L *et al* 2015 Emergence of multiple superconducting phases in $(NH_3)_yM_xFeSe$ ($M = Na$ and Li) *Sci. Rep.* **5** 12774
- [39] Harada I, Kawai R and Kubo Y 2014 Charge density and bonding properties of $LaFeAsO$ under pressure *J. Phys. Soc. Japan* **83** 024716
- [40] Hesani M and Yazdani A 2018 An investigation of the interrelationship between pressure and correlation in $LaFeAsO$ under pressure *Physica C* **553** 38
- [41] Takahashi H, Okada H, Igawa K, Kamihara Y, Hirano M and Hosono H 2009 Pressure studies of $(La, Sm)FeAsO_{1-x}F_x$ and $LaFePO$ *Physica C* **469** 413
- [42] Takahashi H, Tomita T, Soeda H, Ebata M, Okuma K, Hanna T, Muraba Y, Matsuishi S and Hosono H 2012 High-pressure studies for hydrogen substituted $CaFeAsF_{1-x}H_x$ and $SmFeAsO_{1-x}H_x$ *J. Supercond. Nov. Magn.* **25** 1293
- [43] Mizuguchi Y, Hara Y, Deguchi K, Tsuda S, Yamaguchi T, Takeda K, Kotegawa H, Tou H and Takano Y 2010 Anion height dependence of T_c for the Fe-based superconductor *Supercond. Sci. Technol.* **23** 054513
- [44] Kamihara Y, Watanabe T, Hirano M and Hosono H 2008 Iron-based layered superconductor $La[O_{1-x}F_x]FeAs$ ($x = 0.05-0.12$) with $T_c = 26$ K *J. Am. Chem. Soc.* **130** 3296
- [45] Hanna T, Muraba Y, Matsuishi S, Igawa N, Kodama K, Shamoto S and Hosono H 2011 Hydrogen in layered iron arsenides: indirect electron doping to induce superconductivity *Phys. Rev. B* **84** 024521
- [46] Liu R H *et al* 2008 Anomalous transport properties and phase diagram of the FeAs-based $SmFeAsO_{1-x}F_x$ superconductors *Phys. Rev. Lett.* **101** 087001
- [47] Iimura S, Okanishi H, Matsuishi S, Hiraka H, Honda T, Ikeda K, Hansen T C, Otomo T and Hosono H 2017 Large-moment antiferromagnetic order in overdoped high- T_c superconductor $154SmFeAsO_{1-x}D_x$ *Proc. Natl Acad. Sci. USA* **114** E4354